Age-dependent changes of stress and strain in the human heart valve and their relation with collagen remodeling

Acta Biomaterialia 29 (2016) 161–169

Contents lists available at ScienceDirect

Acta Biomaterialia

journal homepage: www.elsevier.com/locate/actabiomat

Age-dependent changes of stress and strain in the human heart valve and their relation with collagen remodeling

P.J.A. Oomen [a,b], S. Loerakker [a,b,*], D. van Geemen [b], J. Neggers [c], M.-J.T.H. Goumans [d], A.J. van den Bogaerdt [e], A.J.J.C. Bogers [e], C.V.C. Bouten [a,b], F.P.T. Baaijens [a,b]

[a] Institute for Complex Molecular Systems, Eindhoven University of Technology, 5600MB Eindhoven, Netherlands
[b] Department of Biomedical Engineering, Eindhoven University of Technology, 5600MB Eindhoven, Netherlands
[c] Department of Mechanical Engineering, Eindhoven University of Technology, 5600MB Eindhoven, Netherlands
[d] Department of Molecular Cell Biology, Leiden University Medical Center, 2300RC Leiden, Netherlands
[e] Department of Cardiothoracic Surgery and Heart Valve Bank, Erasmus Medical Center, 3000CA Rotterdam, Netherlands

ARTICLE INFO

Article history:
Received 28 August 2015
Received in revised form 18 October 2015
Accepted 28 October 2015
Available online 6 November 2015

Keywords:
Heart valves
Collagen remodeling
Tissue engineering
Biomechanics

ABSTRACT

In order to create tissue-engineered heart valves with long-term functionality, it is essential to fully understand collagen remodeling during neo-tissue formation. Collagen remodeling is thought to maintain mechanical tissue homeostasis. Yet, the driving factor of collagen remodeling remains unidentified. In this study, we determined the collagen architecture and the geometric and mechanical properties of human native semilunar heart valves of fetal to adult age using confocal microscopy, micro-indentation and inverse finite element analysis. The outcomes were used to predict age-dependent changes in stress and stretch in the heart valves via finite element modeling. The results indicated that the circumferential stresses are different between the aortic and pulmonary valve, and, moreover, that the stress increases considerably over time in the aortic valve. Strikingly, relatively small differences were found in stretch with time and between the aortic and pulmonary valve, particularly in the circumferential direction, which is the main determinant of the collagen fiber stretch. Therefore, we suggest that collagen remodeling in the human heart valve maintains a stretch-driven homeostasis. Next to these novel insights, the unique human data set created in this study provides valuable input for the development of numerical models of collagen remodeling and optimization of tissue engineering.

Statement of significance

Annually, over 280,000 heart valve replacements are performed worldwide. Tissue engineering has the potential to provide valvular disease patients with living valve substitutes that can last a lifetime. Valve functionality is mainly determined by the collagen architecture. Hence, understanding collagen remodeling is crucial for creating tissue-engineered valves with long-term functionality. In this study, we determined the structural and material properties of human native heart valves of fetal to adult age to gain insight into the mechanical stimuli responsible for collagen remodeling. The age-dependent evolutionary changes in mechanical state of the native valve suggest that collagen remodeling in heart valves is a stretch-driven process.

1. Introduction

It has been known for many years that the form and function of many biological tissues are strongly influenced by mechanical stimuli [1–3]. Numerous cell types remodel their surrounding extracellular matrix in response to changes in mechanical loading [4–7], which has been hypothesized to occur to maintain a certain mechanical homeostasis [1,3]. Yet, there is no consensus as to which mechanical quantity is the driving factor behind the remodeling process. Collagen fibers are one of the key players in the remodeling process, since these proteins are the main load-bearing component of many soft tissues. In particular, collagen fiber orientation and bundle formation through cross-linking [8,9] play a significant role in valvular tissue mechanics. As a

* Corresponding author at: Department of Biomedical Engineering, Eindhoven University of Technology, P.O. Box 513, 5600MB Eindhoven, Netherlands.
E-mail addresses: P.J.A.Oomen@tue.nl (P.J.A. Oomen), S.Loerakker@tue.nl (S. Loerakker).

http://dx.doi.org/10.1016/j.actbio.2015.10.044
1742-7061/

consequence, the architecture of the collagen network has a major influence on the mechanical functionality of soft tissues, as well as on mechanically induced growth and remodeling processes. Therefore, a deeper knowledge of collagen remodeling will greatly benefit our understanding of healthy tissue development as well as pathological adaptations such as seen during fibrosis, aneurysm formation [10] and wound healing [11,12]. Moreover, it is of great interest to the rapidly growing field of tissue engineering, which aims to provide patients with living autologous tissue replacements that have the potential to grow and remodel in response to changes in functional demand [13].

One of the endeavors of this field is the development of tissue-engineered heart valves (TEHVs). Despite promising early results, short-term remodeling often leads to tissue crimp that causes leaflet shortening and, ultimately, valve malfunctioning [14–17]. In order to ensure long-term functionality of TEHVs, understanding and subsequently controlling the collagen remodeling process is of the greatest importance. However, this is impeded by the lack of long-term data due to the early failure of TEHVs.

We aim to identify the driving factor of collagen remodeling in heart valves and have investigated age-dependent changes in human semilunar heart valves. During their lifetime, the geometry and collagen architecture of heart valves change [18–21], which is likely due to temporal changes in hemodynamical conditions [22,19,1]. Still, it remains unknown how these temporal changes are related to valve mechanics, including tissue stress and strain.

Knowledge of the evolutionary changes with age in stress and strain status of human heart valves might explain which of these factors, if any, determines mechanical homeostasis. Therefore, we determined the collagen architecture as well as the geometric and mechanical properties of human semilunar heart valves of fetal to adult age using confocal microscopy, micro-indentation and inverse finite element analysis. The collagen architecture and geometrical and mechanical properties were used to predict age-dependent changes in stress and stretch in the heart valves via finite element modeling.

2. Materials and methods

2.1. Tissue preparation

Sixteen sets of paired cryopreserved healthy human aortic and pulmonary valves of different ages were obtained from Dutch post-mortem donors, given permission for research according to national ethical and regulatory guidelines with written informed consent. These valves were assessed to be unfit for implantation and provided by the Heart Valve Bank Rotterdam (Erasmus University Medical Center, Rotterdam), with ages ranging from 2 months to 53 years old. Of these valves, thirteen pairs were previously studied by Van Geemen [23] and three pairs (2 months, 2 years and 49 (for microscopy only) years old) were analyzed for the first time in this study. The valves were deemed unfit for implantation due to findings that contra-indicated implantation, consisting amongst others of positive bacteriological sampling, serological findings in the donor and other procedural non-conformities that caused rejection of the donor (e.g. sexual risk behavior and/or risks in drug abuse). Additionally, one cryopreserved fetal heart (19 weeks old) was obtained from the department of Molecular Cell Biology, Leiden University Medical Center, Leiden, after approval by the medical ethical committee of the Leiden University Medical Center and written informed consent.

All valves were structurally and mechanically unaffected and the cause of death was not related to valvular disease or conditions known to precede valvular disease. The cryopreserved valves were stored at −80 °C and thawed and prepared just prior to testing, as described previously [23]. Previous studies showed that the applied cryopreservation protocol did not affect structural integrity [24] and mechanical properties [25]. The valves were stained overnight with CNA35 [26] to enable collagen visualization.

2.2. Collagen architecture visualization and quantification

The collagen architecture of a single leaflet of the fetal valve and 2-month, 2-year and 43-year-old valve pairs was visualized using a confocal laser scanning microscope (TCS SP5X, Leica Microsystems, Wetzlar, Germany) with complimentary software (Leica Application Suite Advanced Fluorescence, Leica Microsystems, Wetzlar, Germany). The valves were placed on the microscope such that the fibrosa faced the camera. A tile scan (magnification 10x, excitation 520 nm, emission 488 nm) was made to capture the collagen architecture of the entire leaflet in one single image. Collagen fiber orientation and dispersity were determined by analyzing the individual images of each tile scan, using a custom Mathematica (Wolfram, Champaign, IL, USA) script, based on the work of Frangi et al. [27], which has been used previously to measure collagen orientation [28,29]. In brief, the orientation of collagen fibers was determined via a multi-scale approach in which the principle curvature directions were calculated from the eigenvalues and the eigenvectors of the Hessian matrix of the image (second order derivative). For each tile scan, a histogram containing the fiber fraction per angle was obtained, from which the fiber main orientation and dispersity could be derived using a least-squares fitting method.

2.3. Mechanical testing

One leaflet of each valve was used for mechanical testing using micro-indentation, as described previously [30,31]. A spherical sapphire indenter with a diameter of 2 mm was used. The whole setup was mounted on an Axiovert 200M confocal laser scanning microscope (Carl Zeiss, Oberkochen, Germany) with iXon + camera and complimentary Andor IQ software (Andor, Belfast, Northern Ireland). This setup enabled tracking of the deformation in the bottom plane of the samples during deformation by making images of the collagen fibers (magnification 10x, excitation 520 nm, emission 488 nm) during indentation. Each leaflet was indented at ~7 locations across the belly region, with 3 indentation cycles performed at each location. During each cycle, the leaflet was indented up to 50% of the local leaflet thickness with a constant indentation speed of 0.01 mm/s. The vertical indentation force, planar valve deformation, and thickness were obtained for each cycle, which were averaged to one single data set per leaflet for further analysis. The first cycle was used as pre-conditioning cycle and excluded from further analysis. Mechanical testing of a 11-year-old pediatric pulmonary valve failed due to hardware failure.

2.4. Digital image correlation

A global digital image correlation (GDIC) algorithm was used to quantify deformation in the confocal microscopy images made during indentation. This algorithm was adapted from Neggers et al. in MATLAB (MathWorks, Natick, MA, USA) [32,33]. In brief, the algorithm considers each image as a scalar function of spatial coordinates that gives the gray level at each pixel. The displacement field relating two subsequent images was decomposed onto a basis of continuous functions. The parametrized displacement field was found by incrementally minimizing the squared difference between the two images using a multi-scale approach. For a full scope on the GDIC algorithm and implementation, please be referred to Neggers et al. [33].

2.5. Inverse finite element analysis

With force and strain data available, the material parameters for the constitutive model described in the next section were computed by inverse finite element analysis. Since the indenter was centered directly above the indentation site, quarter-symmetry could be assumed. Therefore, a small block of tissue surrounding the indenter was modeled in the commercial finite element package Abaqus (Dassault Systèmes Simulia Corp., Providence, RI), using ~100 quadratic brick elements with reduced integration (C3D20R). Mesh dimensions were sample-dependent due to differences in sample thickness. Material parameters were estimated by minimizing the difference between the experimental and numerical data, using a quadratic objective function to define the goodness of fit, as described previously [34]. The resulting parameters were used for numerical simulations and are displayed in Table 1.

2.6. Constitutive model

The finite element model is based on the work of Driessen et al. and Loerakker et al. [35,36]. The model was implemented in Abaqus using the user-defined subroutine UMAT. The heart valve leaflet is modeled as a fiber-reinforced composite material, consisting of an anisotropic fiber part (f) with volume fraction (ϕ_f) and an isotropic matrix part (m) with volume fraction ($1-\phi_f$). The fiber volume fraction ϕ_f was set to 0.5, similar to [35]. The total Cauchy stress hence consists of two components:

$$\boldsymbol{\sigma} = \boldsymbol{\sigma}_m + \boldsymbol{\sigma}_f \tag{1}$$

The isotropic part, describing the contribution of the cells and all extracellular matrix components except collagen, is modeled as a Neo-Hookean material:

$$\boldsymbol{\sigma}_m = (1-\phi_f)\left(\kappa\frac{\ln(J)}{J}\boldsymbol{I} + \frac{G}{J}(\boldsymbol{B} - J^{2/3}\boldsymbol{I})\right) \tag{2}$$

with $\boldsymbol{F}$ the deformation gradient tensor, $J = \det(\boldsymbol{F}), \boldsymbol{B} = \boldsymbol{F}\cdot\boldsymbol{F}^T$, and G and κ the shear and compression modulus, respectively. The anisotropic fiber part is modeled using an angular distribution with a discrete number of fiber directions. The fiber directions $\boldsymbol{e}^i_{f0}$ in the undeformed configuration are positioned within a plane spanned by two orthogonal vectors in the circumferential ($\boldsymbol{v}_1$) and radial ($\boldsymbol{v}_2$) direction at angles γ^i with respect to $\boldsymbol{v}_1$:

$$\boldsymbol{e}^i_{f,0} = \cos(\gamma^i)\boldsymbol{v}_1 + \sin(\gamma^i)\boldsymbol{v}_2 \tag{3}$$

The fiber volume fraction in each direction was described using a periodic version of the normal probability distribution function [37,35]:

$$\varphi^i_f = A\exp\left[\frac{\cos[2(\gamma_i-\alpha)]+1}{\beta}\right] \tag{4}$$

where α is the main fiber angle with respect to $\vec{v}_1$ and β the dispersity of the fiber distribution. The scaling factor A is defined such that the total fiber content equals ϕ_f. An angular resolution of 3° was used to model the collagen distribution. The total collagen fiber stress depends on the orientation of the collagen fibers in the current configuration ($\boldsymbol{e}^i_f$) and the collagen stress and volume fraction φ^i_f in each direction:

Table 1
Geometrical, hemodynamic and material parameter values used in all simulations.

						Material parameters			
Age group	Age	Site	Radius (mm)	Thickness (mm)	Pressure[a] (kPa)	G (kPa)	k_1 (kPa)	k_2 (-)	β (-)
Fetal	19w	Pulmonary	1.5	0.21 ± 0.10	1.6	11.1	8.9	0.92	0.58
Pediatric	2 m	Aortic	4.0	0.32 ± 0.05	4.9	5.2	0.30	6.16	0.37
	2 m	Pulmonary	5.0	0.29 ± 0.04	1.1	6.3	0.14	6.92	0.41
	8 m	Aortic	5.0	0.50 ± 0.16	4.9	6.8	0.28	7.54	0.56
	8 m	Pulmonary	5.5	0.28 ± 0.09	1.1	5.0	0.43	5.70	0.73
	2y	Aortic	5.5	0.68 ± 0.02	5.6	11.4	0.10	8.93	0.35
	2y	Pulmonary	6.5	0.52 ± 0.04	1.1	5.0	0.55	4.82	0.43
	5y	Aortic	7.0	0.68 ± 0.11	7.1	53.4	0.10	8.77	0.25
	5y	Pulmonary	9.0	0.60 ± 0.17	1.1	12.8	0.48	3.52	0.53
	11y	Aortic	8.5	0.82 ± 0.27	8.1	24.1	0.26	5.22	0.46
	11y[d]	Pulmonary	8.5	–	1.1	–	–	–	–
Adolescent	18y[b]	Aortic	10.5	1.0 ± 0.44	8.4	13.7	0.28	4.75	0.50
	18y[b]	Pulmonary	11.0	0.32 ± 0.09	1.1	5.0	0.10	7.20	1.67
	18y[c]	Aortic	9.5	0.73 ± 0.24	8.4	10.2	0.21	6.70	0.60
	18y[c]	Pulmonary	13.0	0.28 ± 0.15	1.1	5.0	1.50	2.02	1.26
	20y	Aortic	10.0	0.93 ± 0.16	8.7	9.4	0.66	5.10	0.51
	20y	Pulmonary	10.0	0.48 ± 0.13	1.1	5.0	0.43	4.85	1.02
	22y	Aortic	9.5	0.80 ± 0.25	8.7	10.7	2.01	3.36	0.66
	22y	Pulmonary	9.5	0.34 ± 0.13	1.1	5.0	8.92	1.32	1.07
Adult	38y	Aortic	10.5	0.48 ± 0.38	10.6	15.1	0.10	11.3	0.26
	38y	Pulmonary	10.5	0.27 ± 0.14	1.1	5.0	0.91	5.51	0.45
	40y	Aortic	11.0	0.64 ± 0.20	10.6	11.1	0.10	12.6	0.28
	40y	Pulmonary	12.5	0.25 ± 0.02	1.1	5.0	1.69	4.58	0.68
	47y	Aortic	13.0	0.54 ± 0.17	10.6	35.8	0.20	10.8	0.31
	48y	Aortic	11.0	0.69 ± 0.14	10.6	9.7	1.64	5.93	0.50
	48y	Pulmonary	13.5	0.27 ± 0.07	1.1	5.0	1.63	4.23	0.46
	51y[e]	Aortic	11.0	0.67 ± 0.31	10.6	–	–	–	0.27
	51y	Pulmonary	11.0	0.36 ± 0.16	1.1	6.1	0.25	9.36	0.34
	53y[e]	Aortic	11.5	0.68 ± 0.32	10.6	–	–	–	0.22
	53y	Pulmonary	13.0	0.38 ± 0.18	1.1	5.0	0.18	7.47	0.36

[b,c] Paired 18-year-old valves.
[a] References for diastolic pressure magnitudes: fetal [38], pediatric aortic [39], adolescent aortic [40], adult aortic [41] and pulmonary [41].
[d] Hardware failure occurred during mechanical testing.
[e] No convergence was reached in the inverse analysis.

$$\boldsymbol{\sigma}_f = \sum_{i=1}^{N} \varphi_f^i \sigma_f^i \boldsymbol{e}_f^i \boldsymbol{e}_f^i \tag{5}$$

with σ_f^i the magnitude of the fiber stress depending on the fiber stretch λ_f. An exponential stress-stretch law with stiffness parameters k_1 and k_2 was used for the fiber stress when the collagen fibers are extended ($\lambda_f^i \geqslant 1$) [35]. It is assumed that collagen fibers can only bear stress in extension, with a small compressive stress when $\lambda_f^i < 1$ to prevent numerical convergence issues due to discontinuities in fiber stress derivatives:

$$\sigma_f^i = \begin{cases} k_1 (\lambda_f^i)^2 \left(e^{k_2((\lambda_f^i)^2 - 1)} - 1 \right) & , \lambda_f^i \geqslant 1 \\ \frac{k_1 k_2}{k_3} \left(e^{k_3((\lambda_f^i)^2 - 1)} - 1 \right) & , \lambda_f^i < 1 \end{cases} \tag{6}$$

where $\lambda_f^i = \sqrt{\boldsymbol{e}_{f0}^i \cdot \boldsymbol{F}^T \cdot \boldsymbol{F} \cdot \boldsymbol{e}_{f0}^i}$ is the stretch in fiber direction $\boldsymbol{e}_i$.

2.7. Finite element meshes

Each valve was shaped by creating spherical leaflets using age-related geometrical properties (Table 1). Only half of one leaflet was modeled due to symmetry and divided into ~500 quadratic brick elements with reduced integration (C3D20R). Mesh refinement was applied such that the mesh density was higher in the belly region. For every element, the radial direction was defined as the vector perpendicular to the outer normal of the element $\boldsymbol{n}$ and a unit vector in $\boldsymbol{x}$-direction $\boldsymbol{e}_x$: $\boldsymbol{v}_2 = (\boldsymbol{e}_x \times \boldsymbol{n}) / \| \boldsymbol{e}_x \times \boldsymbol{n} \|$. Subsequently, the circumferential direction was calculated as $\boldsymbol{v}_1 = \boldsymbol{n} \times \boldsymbol{v}_2$ [36].

2.8. Analyses

Simulations were performed using the age-related geometrical, hemodynamic and material properties measured in fetal, pediatric, adolescent and adult valves (Table 1). The age-related diastolic blood pressure was gradually applied. Circumferential and radial stretch and Cauchy stress were computed in the belly region.

3. Results

3.1. Collagen architecture evolution is a multi-scale process

High-resolution confocal microscopy images were obtained from the fibrosa side of one pulmonary fetal leaflet and paired aortic and pulmonary leaflets aged 2 months, 2 years and 49 years (Fig. 1). At the microscopic scale, quantification of the individual collagen fiber orientation revealed a circumferential main orientation in all valves, including the fetal valve. Across all ages, the fiber dispersity of the aortic valves was lower than their complementing pulmonary valves (Fig. 2). However, due to relatively large inter-patient variation in dispersity, particularly for the pulmonary valve, no temporal trends in fiber dispersity could be observed in both valve types.

On the macroscopic level, the postnatal architecture of the fibrosa of both the aortic and pulmonary leaflets was characterized by bundles of densely packed circumferentially oriented collagen fibers. No fiber bundles were visible in the fetal valve; bundles of limited size were observed in the 2-month-old and 2-year-old valves and larger bundles were present in the adult heart valve, in particular in the aortic valve. These observations suggest that the fiber bundles develop with time.

3.2. Valve stiffness increases as a function of age

The mechanical properties of the valvular tissue were quantified using a combination of, micro-indentation[31], digital image correlation [33] and inverse finite element analysis [34]. The resulting parameters for each individual valve can be found in (Table 1). Unfortunately, the parameter estimation algorithm did not converge for three adult aortic valves.

One should be careful in directly comparing the material parameters from different valves, as different combinations of parameters could give a similar result. To compare the mechanical

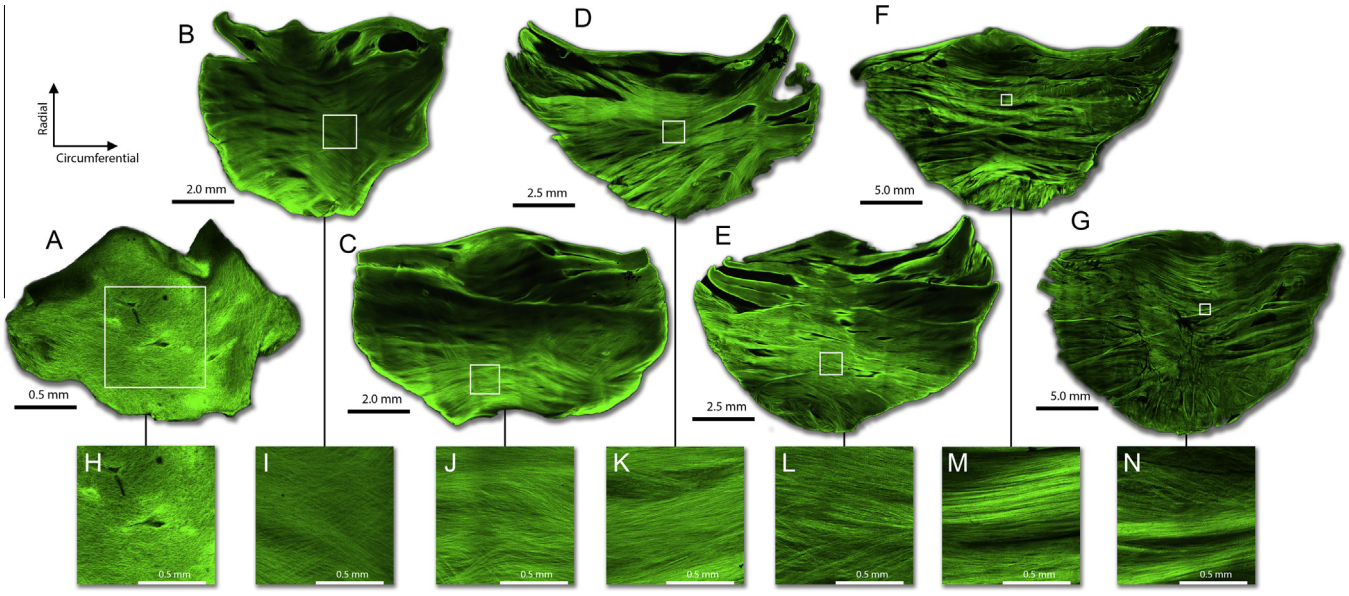

Fig. 1. Collagen fiber architectures of human native heart valve leaflets' fibrosa side of a fetal pulmonary valve (A) and three valve pairs: 2-month-old aortic (B) and pulmonary (C), 2-year-old aortic (D) and pulmonary (E) and 49-year-old aortic (F) and pulmonary valves (G). Bundles of densely packed collagen fibers are visible postnatally and appear to arise with age, with individual fibers depicted in the insets (H-N). A mainly circumferentially oriented collagen architecture was found in all valves.

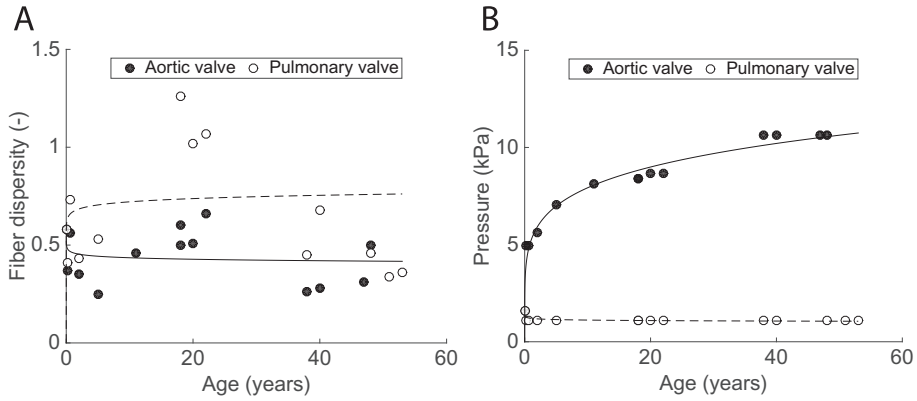

Fig. 2. Age-related changes in fiber dispersity (A) and diastolic blood pressure (B) in the aortic and pulmonary valve. Fiber dispersity was lower in the aortic valve than in the pulmonary valve and power law trend lines indicate the temporal evolution of both pressure and fiber dispersity. Fiber dispersity remains approximately constant as a function of age, however a large spread in the data was observed. Diastolic blood pressure in the aortic valve increases rapidly postnatally, [38,39], whereas in the pulmonary circulation a slight drop in pressure occurs [41].

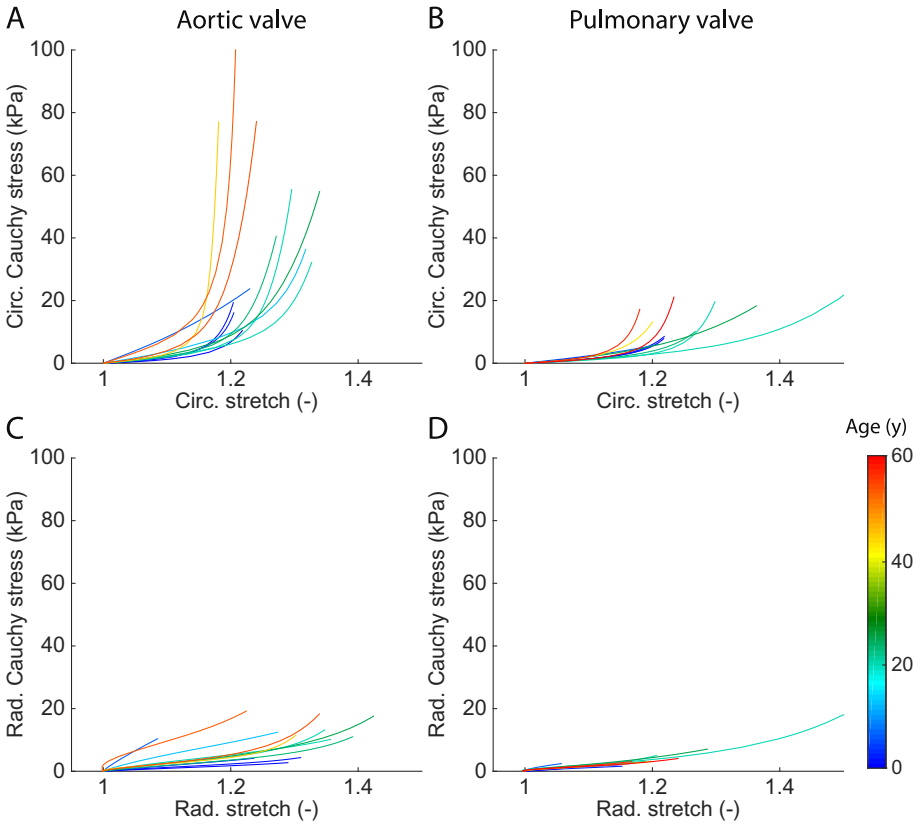

Fig. 3. Stress-stretch curves in the circumferential (A, B) and radial (C, D) direction in the belly region of the aortic and pulmonary valve simulations. Valve stiffness in the circumferential direction increased as a function of age for both aortic and pulmonary valve.

properties of the different valves, it is better to focus on the stress-stretch curves for each valve simulation. These curves (Fig. 3) show that the aortic valves were stiffer than the pulmonary valves in the circumferential direction. Moreover, a temporal increase of circumferential stiffness was observed in both valves, whereas no such trend could be observed for the radial direction.

3.3. Age-related simulations point to stretch homeostasis and not stress homeostasis

The mechanical state of the different valves was simulated using finite element modeling [35,36] incorporating the experimentally obtained data (Table 1). The diastolic pressure corresponding with each age and location (Fig. 2) was applied to the arterial side of the valve and the stretch ratio and Cauchy stress were computed in the circumferential and radial direction. Unfortunately, no convergence was reached for five valves (three aortic, two pulmonary), which were excluded from further analysis. Significant changes in leaflet stretch were predicted in the belly region at young age (<4 years), followed by a stretch homeostasis in both the aortic and pulmonary valve (Fig. 4A and C). Strikingly, this circumferential stretch homeostasis was similar for the aortic and pulmonary valves. On the other hand, the radial stretch in the aortic valves was higher than in their pulmonary counterparts,

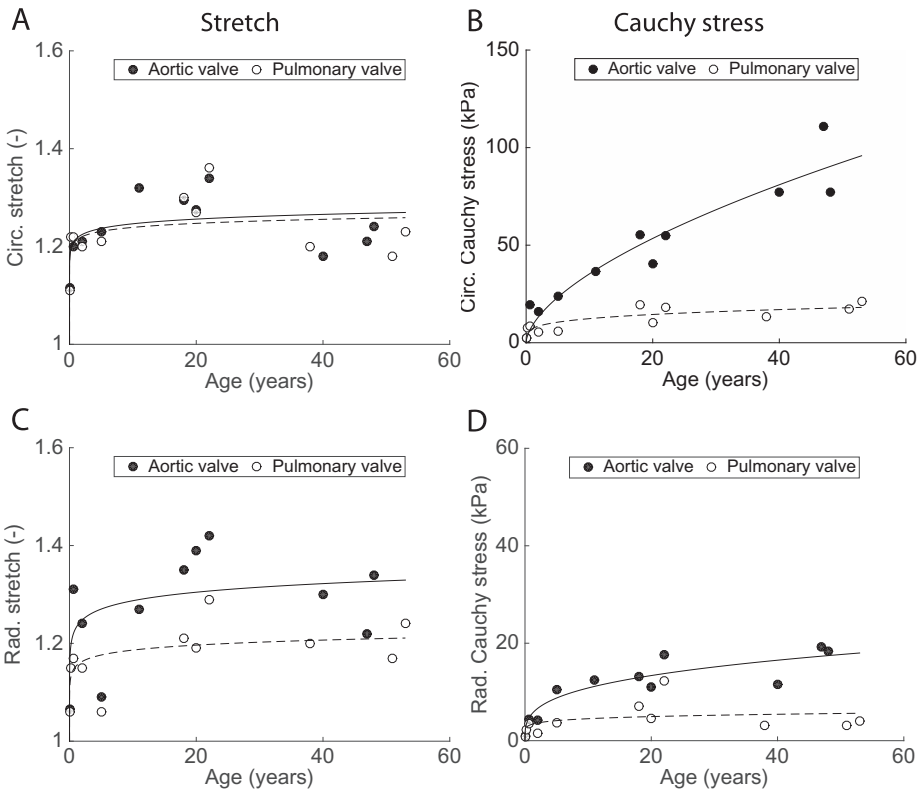

Fig. 4. Circumferential (A, B) and radial (C, D) stretch ratios and stresses in the belly region for aortic and pulmonary heart valves after full coaptation. Power law trend lines were fitted using least squares to indicate the temporal trends for both valves. Circumferential stretch was similar in the aortic and pulmonary valves, whereas the radial stretch and circumferential and radial stress were larger in the aortic valve.The simulations for the 2-month, 18-year and 38-year-old aortic valves and 18-year and 40-year-old pulmonary valves failed to converge.

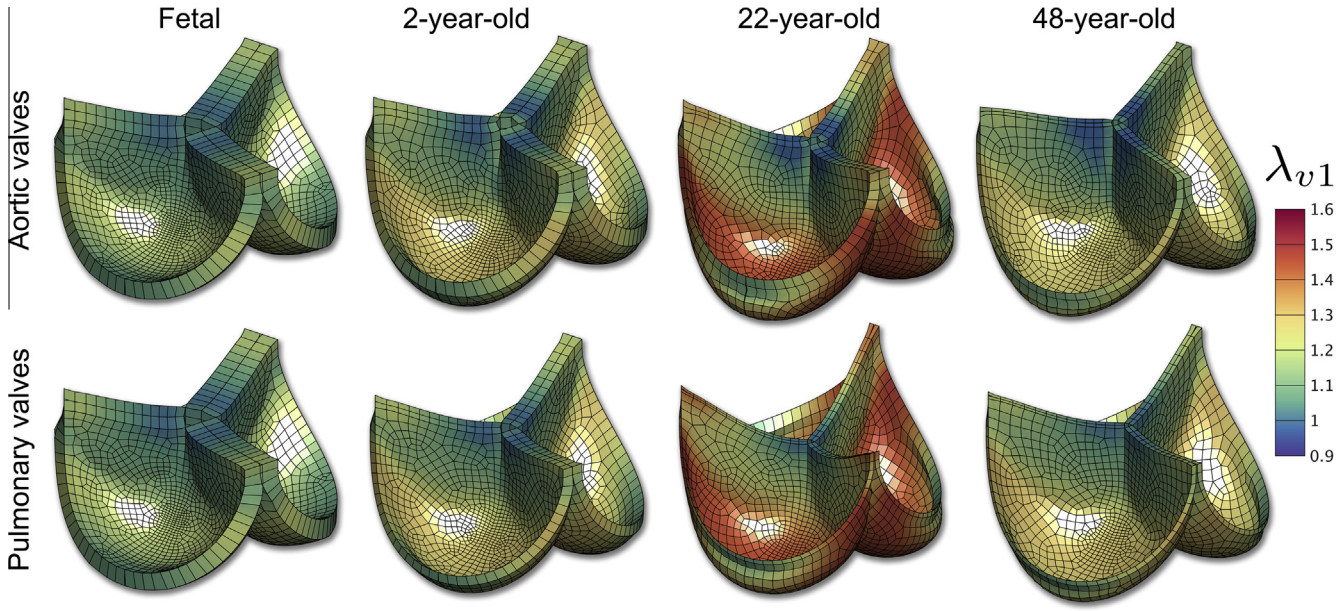

Fig. 5. Circumferential stretch (λ_{v_1}) distributions estimated by the numerical models of four selected valve pairs (fetal, 2-year-old, 22-year old and 48-year-old) after full coaptation. The stretches were similar between the aortic and pulmonary valves across all ages. In this figure, the scaled to the same size to enable comparison between valves of different ages.

which can be explained by the higher aortic blood pressure in combination with the limited amount of radially oriented collagen fibers.

The circumferential stretch field is shown for selected valves of different ages in Fig. 5. Slight differences can be observed between valves of different donors, for example a higher stretch in the

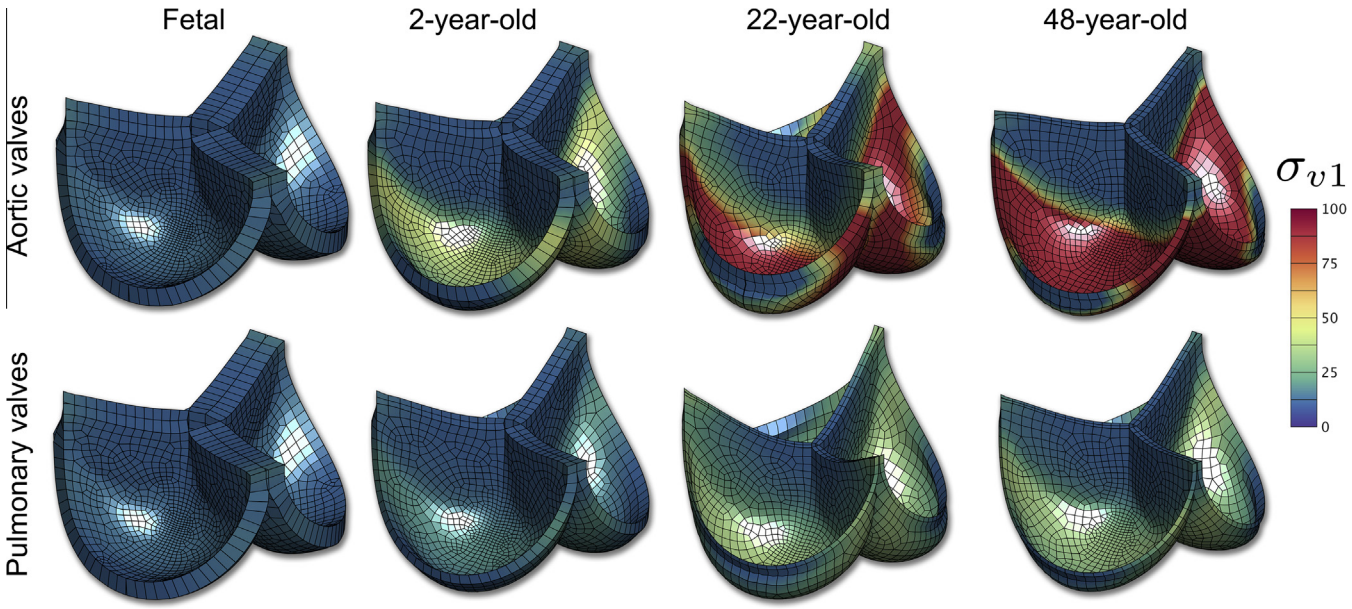

Fig. 6. Circumferential stress (σ_{v_1}) distributions estimated by the numerical models of four selected valve pairs (fetal, 2-year-old, 22-year old and 48-year-old) after full coaptation. The circumferential stress in the aortic valves increased with age, whereas in the pulmonary valve no significant changes were observed. In this figure, the scaled to the same size to enable comparison between valves of different ages.

22-year-old valves compared to valves from other donors. Yet, aortic and pulmonary valves of the same donor feature a similar stretch field.

In contrast to the circumferential leaflet stretch, no homeostasis was predicted for the circumferential Cauchy stress in the aortic valve, with stress continuously increasing with age (Fig. 4B). The values and changes in stress in the pulmonary valve were relatively small compared to the aortic valve, which may be due to the low pulmonary blood pressure that hardly changes with age. The circumferential stress field is shown for selected valves of different ages in Fig. 6. The radial stress in both valve types was smaller than the circumferential stress (Fig. 4D), which can be explained by the circumferential alignment of the collagen fibers.

Due to the circumferential alignment of the collagen fibers, these results suggest that collagen remodeling ensures that the stretches in the collagen fibers are similar in the aortic and pulmonary valve across all ages. In contrast, the circumferential stress is different between the two valves and increases with time in the aortic valve. Therefore, these data suggest that collagen remodeling aims to maintain a constant collagen stretch.

4. Discussion

For the first time, human heart valves of different ages were used to reveal age-related changes in valve stress and stretch status, as well as geometry and collagen architecture. The data suggests that these changes may be related to collagen remodeling in response to changes in hemodynamics, in order to maintain a stretch-driven mechanical homeostasis.

4.1. Collagen remodeling is a stretch-driven phenomenon

Age-dependent finite element simulations predicted small differences in stretch with age and between the aortic and pulmonary valve leaflets, especially in the circumferential direction (Fig. 4A and C). As the collagen fibers are mainly oriented in this direction, this would suggest that collagen remodeling aligns collagen fibers to prevent excessive tissue stretch that occurs due to the increasing diastolic blood pressure (Fig. 2B).

In contrast, no stress homeostasis was found in the circumferential direction, with the stress continuously increasing with age (Fig. 2B). This increase in circumferential stress as a consequence of rising blood pressure was apparently not counteracted by growth and remodeling. A stress homeostasis could for instance have been maintained by tissue thickening. However, the increase in thickness in the aortic valve with time and in comparison with the pulmonary valve appears to be insufficient to prevent the increase in stress with age, thus making it less likely that collagen remodeling is stress-driven.

In the present study, we studied collagen remodeling at the tissue level. In order to fully unravel the underlying mechanisms of collagen remodeling, it needs to be included how the cells sense and respond to mechanical changes in their environment [3]. Recently, computational models were proposed that describe the interaction between cellular traction forces and collagen remodeling which may shed light on these mechanisms [42,43]. The findings of the present study can be valuable for developing these kind of models, in order to eventually develop a full understanding of the collagen remodeling mechanism.

4.2. Collagen remodeling can be attributed to changes in hemodynamics

The high spatial resolution of the confocal images in this study allowed for fiber architecture analysis and quantification on multiple scales: from dense fiber bundles on the macroscopic level, up to individual fiber distributions on the microscale (Fig. 1). All valves that were measured featured a main circumferential fiber orientation, which is consistent with previous findings [44–47]. Most interestingly, the temporal evolution of the collagen architecture appears to feature different phenomena across the scales. This evolution can be related to temporal changes in hemodynamics, as well as differences in blood pressure between the aortic and pulmonary circulation.

At the microscale, the collagen alignment was higher in the aortic valve than in the pulmonary valve, which can be explained by remodeling in response to changes in hemodynamics. The postnatal rise in aortic blood pressure primarily leads to an increase in

circumferential stretch in case of isotropic collagen networks [48,36]. Consequently, tissue remodeling in the aortic valve leads to a stronger alignment of the collagen network in the circumferential direction in order to decrease the circumferential stretch and maintain the stretch homeostasis.

Hemodynamics can also explain the large inter-patient variability in fiber dispersity that was observed in the pulmonary valve. Due to the highly nonlinear stress-stretch behavior of collagen fibers, the fibers will not be fully stretched at a low pressure. This implies that the collagen alignment is less crucial to maintain the stretch homeostasis in the pulmonary valve, as the blood pressure is much lower than in the aortic valve. Therefore, the collagen fiber dispersity in the pulmonary valves can be higher and more diverse than in the aortic valves.

In contrast to the microscopic scale, the collagen architecture at the macroscopic scale evolves with time. Bundles of densely packed collagen fibers are visible in postnatal valves and become more pronounced in the older valves, which concurs with previous findings [19]. Since these bundles were found in both the aortic and pulmonary valve, their formation does not only appear to be induced by changes in leaflet stretch but may also be an effect of ageing.

4.3. Valve stiffness is adapted by collagen remodeling to prevent excessive stretching

Several studies have characterized the mechanical behavior of heart valves [49–54]. Yet, to the best of the authors' knowledge, this is the first time that the mechanical properties of human semilunar heart valves of life-spanning age groups were quantified. The micro-indentation technique combined with inverse finite element analysis that was employed in this study has previously been used for characterizing anisotropic biological tissues [34,31,55]. The main advantage of micro-indentation compared to for example biaxial tensile testing is that it can measure even the smallest samples, thus enabling mechanical characterization of the fetal and pediatric valves included in this study.

As collagen is the main load-bearing component of heart valves, changes in valve stiffness can be related to changes of the collagen architecture with age and between the aortic and pulmonary valve. The higher stiffness in the aortic compared to the pulmonary valve (Fig. 3) can be explained by the lower fiber dispersity in the aortic valve. On the other hand, the fiber dispersity remains constant with time and the total collagen content is known to remain unchanged after childhood [19]. Therefore, the temporal increase in circumferential stiffness and nonlinearity can only be due to fiber bundle formation. Hence, fiber bundle formation influences valve mechanics by providing additional tissue stiffness, even though it may not be merely modulated by changes in mechanical loading.

4.4. Limitations

The use of unique human data to gain novel insights in valve tissue remodeling yields two main limitations. First, due to the limited availability, the sample number was low. This can for example explain the stretch variations between valves from different donors (Fig. 5) and the spread in fiber dispersity (Fig. 2). These variations can amongst others be caused by deviating hemodynamics. For example, the high stretch that was predicted in the 22-year-old valve (Figs. 4A, C and 5) could be due to the donor being hypotensive, leading to a lower stiffness due to decreased mechanical demand and hence a higher stretch when normotensive conditions are assumed in the model.

Second, the stresses and stretches that were found in this study (Figs. 4–6) may be underestimated due to in vivo pre-stretches and residual stresses that are present in many biological tissues [56–59]. In aortic and pulmonary heart valve leaflets they can be attributed to the cell tension in the leaflets themselves and pre-stretch and residual stresses in the aortic root. After dissection of the leaflets from the aortic root and cell death, these residual stresses were eliminated. Hence, mechanical characterization took place in a stress-free state. Yet, in our numerical simulations, the unloaded reference state was regarded as stress-free because the in vivo residual stresses could not be measured.

4.5. Implications for tissue engineering

In order to ensure long-term functionality of TEHVs, understanding and controlling the collagen remodeling process is of the greatest importance. However, long-term data is currently unavailable. In the current study, we aimed to identify the driving force of collagen remodeling by studying the evolution of stress and strain status in the human semilunar heart valves. By using heart valves of wide-ranging ages, different time points were obtained in the evolution of the human heart valve, which provided insight in the remodeling process. Additionally, the unique human data set created in this study is a valuable tool for developing future numerical collagen remodeling models that can predict the temporal changes observed in the present study.

Our results indicated that the circumferential stresses are different between the aortic and pulmonary valve, and, moreover, that the stress increases considerably over time in the aortic valve. In contrast, we found relatively small differences in valvular stretch with age and between the aortic and pulmonary valve, particularly in the circumferential direction, which is the main determinant of the stretch experienced by the collagen fibers. Therefore, we suggest that collagen remodeling in the human heart valve maintains a stretch-driven homeostasis.

Tissue engineers can take these findings into account in the design of TEHVs, for instance by adapting scaffold material, geometry and fiber alignment [36] to ensure that a developing tissue will be continuously exposed to a homeostatic stretch. This can direct the cells into functional regeneration of heart valve tissue while simultaneously preventing leaflet fibrosis. Once the collagen remodeling process can be predicted and controlled, long-term functionality of tissue-engineered heart valves can be ensured, thus providing patients with a heart valve that will last for a lifetime.

Disclosures

The authors have declared that no conflicts of interests exist.

Acknowledgements

The research leading to these results has received funding from the European Union's Seventh Framework Programme under Grant agreements n° 242008 and 604514.

References

[1] J.D. Humphrey, Vascular adaptation and mechanical homeostasis at tissue, cellular, and sub-cellular levels, Cell Biochem. Biophys. 50 (2) (2008) 53–78.
[2] D. Ambrosi, G. Ateshian, E. Arruda, S. Cowin, J. Dumais, A. Goriely, G. Holzapfel, J. Humphrey, R. Kemkemer, E. Kuhl, J. Olberding, L. Taber, K. Garikipati, Perspectives on biological growth and remodeling, J. Mech. Phys. Solids 59 (4) (2011) 863–883.
[3] J.D. Humphrey, E.R. Dufresne, M.A. Schwartz, Mechanotransduction and extracellular matrix homeostasis, Nat. Rev. Mol. Cell Biol. 15 (12) (2014) 802–812.
[4] D.Y. Leung, S. Glagov, M.B. Mathews, Cyclic stretching stimulates synthesis of matrix components by arterial smooth muscle cells in vitro, Science 191 (4226) (1976) 475–477.

[5] C. Huang, I.V. Yannas, Mechanochemical studies of enzymatic degradation of insoluble collagen-fibers, J. Biomed. Mater. Res. 11 (1) (1977) 137–154.
[6] R.T. Prajapati, B. Chavally-Mis, D. Herbage, M. Eastwood, R.A. Brown, Mechanical loading regulates protease production by fibroblasts in three-dimensional collagen substrates, Wound Repair Regener. 8 (3) (2000) 226–237.
[7] J.W. Ruberti, N.J. Hallab, Strain-controlled enzymatic cleavage of collagen in loaded matrix, Biochemical and biophysical research communications 336 (2) (2005) 483–489.
[8] A. Balguid, M.P. Rubbens, A. Mol, R.A. Bank, A.J.J.C. Bogers, J.P. Van Kats, B.A.J.M. De Mol, F.P.T. Baaijens, C.V.C. Bouten, The role of collagen cross-links in biomechanical behavior of human aortic heart valve leaflets – relevance for tissue engineering, Tissue Eng. 13 (7) (2007) 1501–1511.
[9] I.G. Aldous, J.M. Lee, S.M. Wells, Differential changes in the molecular stability of collagen from the pulmonary and aortic valves during the fetal-to-neonatal transition, Ann. Biomed. Eng. 38 (9) (2010) 3000–3009.
[10] G. Martufi, T.C. Gasser, Turnover of fibrillar collagen in soft biological tissue with application to the expansion of abdominal aortic aneurysms, J. R. Soc. Interface 9 (77) (2012) 3366–3377.
[11] J.M. McPherson, K.A. Piez, Collagen in dermal wound repair, in: The Molecular and Cellular Biology of Wound Repair, Springer, US, Boston, MA, 1988, pp. 471–496.
[12] K.S. Midwood, L.V. Williams, J.E. Schwarzbauer, Tissue repair and the dynamics of the extracellular matrix, Int. J. Biochem. Cell Biol. 36 (6) (2004) 1031–1037.
[13] R. Langer, J.P. Vacanti, Tissue engineering, Science 260 (5110) (1993) 920–926.
[14] S.P. Hoerstrup, R. Sodian, S. Daebritz, J. Wang, Functional living trileaflet heart valves grown in vitro, Circulation 102 (2000) III44–III49.
[15] D. Schmidt, P.E. Dijkman, A. Driessen-Mol, R. Stenger, C. Mariani, A. Puolakka, M. Rissanen, T. Deichmann, B. Odermatt, B. Weber, M.Y. Emmert, G. Zund, F.P. Baaijens, S.P. Hoerstrup, Minimally-invasive implantation of living tissue engineered heart valves: a comprehensive approach from autologous vascular cells to stem cells, J. Am. Coll. Cardiol. 56 (6) (2010) 510–520.
[16] D. Gottlieb, T. Kunal, S. Emani, E. Aikawa, D.W. Brown, A.J. Powell, A. Nedder, G. C. Engelmayr, J.M. Melero-Martin, M.S. Sacks, J.E. Mayer, In vivo monitoring of function of autologous engineered pulmonary valve, J. Thorac. Cardiovasc. Surg. 139 (3) (2010) 723–731.
[17] A. Driessen-Mol, M.Y. Emmert, P.E. Dijkman, L. Frese, B. Sanders, B. Weber, N. Cesarovic, M. Sidler, J. Leenders, R. Jenni, J. Grünenfelder, V. Falk, F.P. Baaijens, S.P. Hoerstrup, Transcatheter implantation of homologous off-the-shelf tissue-engineered heart valves with self-repair capacity: long-term functionality and rapid in vivo remodeling in sheep, J. Am. Coll. Cardiol. 63 (13) (2014) 1320–1329.
[18] B.J. Maron, G.M. Hutchins, The development of the semilunar valves in the human heart, Am. J. Pathol. 74 (2) (1974) 331–344.
[19] E. Aikawa, P. Whittaker, M. Farber, K. Mendelson, R. Padera, M. Aikawa, F. Schoen, Human semilunar cardiac valve remodeling by activated cells from fetus to adult: implications for postnatal adaptation, pathology, and tissue engineering, Circulation 113 (10) (2006) 1344–1352.
[20] W.J. Larsen, Larsen's Human Embryology, fifth ed., Churchill Livingstone, Philidelphia, 2015.
[21] F. Tongprasert, K. Srisupundit, S. Luewan, S. Sirichotiyakul, W. Piyamongkol, C. Wanapirak, T. Tongsong, Reference ranges of fetal aortic and pulmonary valve diameter derived by STIC from 14 to 40 weeks of gestation, Prenat. Diagn. 31 (5) (2011) 439–445.
[22] E. Rabkin-Aikawa, M. Farber, M. Aikawa, F.J. Schoen, Dynamic and reversible changes of interstitial cell phenotype during remodeling of cardiac valves, J. Heart Valve Dis. 13 (5) (2004) 841–847.
[23] D. Van Geemen, Tissue properties and collagen remodeling in heart valve tissue engineering (Ph.D. Thesis), Technische Universiteit Eindhoven, 2012.
[24] C.J. Gerson, S. Goldstein, A.E. Heacox, Retained structural integrity of collagen and elastin within cryopreserved human heart valve tissue as detected by two-photon laser scanning confocal microscopy, Cryobiology 59 (2) (2009) 171–179.
[25] J.O. Virues, S. Delgadillo, Effect of freezing on the biaxial mechanical properties of arterial samples, J. Biomed. Sci. Eng. 3 (2010) 645–652.
[26] R.A. Boerboom, K.N. Krahn, R.T. Megens, M.A. van Zandvoort, M. Merkx, C.V. Bouten, High resolution imaging of collagen organisation and synthesis using a versatile collagen specific probe, J. Struct. Biol. 159 (3) (2007) 392–399.
[27] A.F. Frangi, W.J. Niessen, K.L. Vincken, M.A. Viergever, Multiscale vessel enhancement filtering, Med. Image Comput. Comput.-Assist. Intervention 1496 (1998) 130–137.
[28] J. Foolen, V.S. Deshpande, F.M.W. Kanters, F.P.T. Baaijens, The influence of matrix integrity on stress-fiber remodeling in 3D, Biomaterials 33 (30) (2012) 7508–7518.
[29] N. De Jonge, F.M.W. Kanters, F.P.T. Baaijens, C.V.C. Bouten, Strain-induced collagen organization at the micro-level in fibrin-based engineered tissue constructs, Ann. Biomed. Eng. 41 (4) (2013) 763–774.
[30] V. Vaenkatesan, Z. Li, W.-P. Vellinga, W.H. de Jeu, Adhesion and friction behaviours of polydimethylsiloxane – a fresh perspective on JKR measurements, Polymer 47 (25) (2006) 8317–8325.
[31] M.A.J. Cox, N.J.B. Driessen, R.A. Boerboom, C.V.C. Bouten, F.P.T. Baaijens, Mechanical characterization of anisotropic planar biological soft tissues using finite indentation: experimental feasibility, J. Biomech. 41 (2) (2008) 422–429.
[32] G. Besnard, F. Hild, S. Roux, Finite-element displacement fields analysis from digital images: application to Portevin–Le Châtelier bands, Exp. Mech. 46 (2006) 789–803.
[33] J. Neggers, J.P.M. Hoefnagels, F. Hild, S. Roux, M.G.D. Geers, A global digital image correlation enhanced full-field bulge test method, Exp. Mech. 54 (2014) 717–727.
[34] M.A.J. Cox, N.J.B. Driessen, C.V.C. Bouten, F.P.T. Baaijens, Mechanical characterization of anisotropic planar biological soft tissues using large indentation: a computational feasibility study, J. Biomech. Eng. 128 (3) (2006) 428–436.
[35] N.J.B. Driessen, A. Mol, C.V.C. Bouten, F.P.T. Baaijens, Modeling the mechanics of tissue-engineered human heart valve leaflets, J. Biomech. 40 (2) (2007) 325–334.
[36] S. Loerakker, G. Argento, C.W.J. Oomens, F.P.T. Baaijens, Effects of valve geometry and tissue anisotropy on the radial stretch and coaptation area of tissue-engineered heart valves, J. Biomech. 46 (11) (2013) 1792–1800.
[37] T.C. Gasser, R.W. Ogden, G.A. Holzapfel, Hyperelastic modelling of arterial layers with distributed collagen fibre orientations, J. R. Soc. Interface 3 (6) (2006) 15–35.
[38] P.C. Struijk, V.J. Mathews, T. Loupas, P.A. Stewart, E.B. Clark, E.A.P. Steegers, J. W. Wladimiroff, Blood pressure estimation in the human fetal descending aorta, Ultrasound Obstet. Gynecol. 32 (5) (2008) 673–681.
[39] NIH, The Fourth Report on Diagnosis, Evaluation, and Treatment of High Blood Pressure in Children and Adolescents, Tech. Rep., institution U.S. Department of Health and Human Services, 2005.
[40] J.D. Wright, J.P. Hughes, Y. Ostchega, S.S. Yoon, T. Nwankwo, Mean systolic and diastolic blood pressure in adults aged 18 and over in the United States, 2001–2008, Nat. Health Stat. Rep. 35 (2011) 1–24.
[41] D. Silverthorn, B. Johnson, Human Physiology: An Integrated Approach, fifth ed., Pearson/Benjamin Cummings, 2010.
[42] V.S. Deshpande, R.M. McMeeking, A.G. Evans, A model for the contractility of the cytoskeleton including the effects of stress-fibre formation and dissociation, Proc. R. Soc. A 463 (2079) (2007) 787–815.
[43] S. Loerakker, C. Obbink-Huizer, F.P.T. Baaijens, A physically motivated constitutive model for cell-mediated compaction and collagen remodeling in soft tissues, Biomech. Model. Mechanobiol. 13 (5) (2014) 985–1001.
[44] A.A. Sauren, W. Kuijpers, A.A. van Steenhoven, F.E. Veldpaus, Aortic valve histology and its relation with mechanics-preliminary report, J. Biomech. 13 (2) (1980) 97–104.
[45] M.S. Sacks, D.B. Smith, E.D. Hiester, The aortic valve microstructure: effects of transvalvular pressure, J. Biomed. Mater. Res. 41 (1) (1998) 131–141.
[46] P.E. Hammer, C.A. Pacak, R.D. Howe, P.J. del Nido, Straightening of curved pattern of collagen fibers under load controls aortic valve shape, J. Biomech. 47 (2) (2014) 341–346.
[47] C.A. Rock, L. Han, T.C. Doehring, Complex collagen fiber and membrane morphologies of the whole porcine aortic valve, PLOS ONE 9 (1) (2014) e86087.
[48] R. Fan, A.S. Bayoumi, P. Chen, C.M. Hobson, W.R. Wagner, J.E. Mayer, M.S. Sacks, Optimal elastomeric scaffold leaflet shape for pulmonary heart valve leaflet replacement, J. Biomech. 46 (4) (2013) 662–669.
[49] K.L. Billiar, M.S. Sacks, Biaxial mechanical properties of the natural and glutaraldehyde treated aortic valve cusp – Part I: experimental results, J. Biomech. Eng. 122 (1) (2000) 23–30.
[50] K.L. Billiar, M.S. Sacks, Biaxial mechanical properties of the native and glutaraldehyde-treated aortic valve cusp: Part II – a structural constitutive model, J. Biomech. Eng. 122 (4) (2000) 327–335.
[51] P. Stradins, R. Lacis, I. Ozolanta, B. Purina, V. Ose, L. Feldmane, V. Kasyanov, Comparison of biomechanical and structural properties between human aortic and pulmonary valve, Eur. J. Cardiothorac. Surg. 26 (3) (2004) 634–639.
[52] C. Martin, W. Sun, Biomechanical characterization of aortic valve tissue in humans and common animal models, J. Biomed. Mater. Res. 100A (6) (2012) 1591–1599.
[53] V. Kasyanov, R. Moreno-Rodriguez, M. Kalejs, I. Ozolanta, P. Stradins, X. Wen, H. Yao, V. Mironov, Age-related analysis of structural, biochemical and mechanical properties of the porcine mitral heart valve leaflets, Connect Tissue Res. 54 (6) (2013) 394–402.
[54] A. Hasan, K. Ragaert, W. Swieszkowski, Š. Selimović, A. Paul, G. Camci-Unal, M. R.K. Mofrad, A. Khademhosseini, Biomechanical properties of native and tissue engineered heart valve constructs, J. Biomech. 47 (9) (2014) 1949–1963.
[55] C.-K. Chai, L. Speelman, C.W.J. Oomens, F.P.T. Baaijens, Compressive mechanical properties of atherosclerotic plaques–indentation test to characterise the local anisotropic behaviour, J. Biomech. 47 (4) (2014) 784–792.
[56] C.J. Chuong, Y.C. Fung, On residual stresses in arteries, J. Biomech. Eng. 108 (2) (1986) 189.
[57] Y.C. Fung, What are the residual stresses doing in our blood vessels?, Ann Biomed. Eng. 19 (3) (1991) 237–249.
[58] A. Delfino, N. Stergiopulos, J. Moore, J.-J. Meister, Residual strain effects on the stress field in a thick wall finite element model of the human carotid bifurcation, J. Biomech. 30 (8) (1997) 777–786.
[59] M.K. Rausch, E. Kuhl, On the effect of prestrain and residual stress in thin biological membranes, J. Mech. Phys. Solids 61 (9) (2013) 1955–1969.